POES/METOP SEM-2 OMNI Flux

Algorithm Theory and Software Description

Revision Record			
Version	**Document Release Date**	**Revision/Change Description**	**Pages Affected**
1.0	03/27/2012	Initial Release – Janet Machol (NOAA/NGDC)	All

TABLE OF CONTENTS

LIST OF FIGURES

LIST OF TABLES

LIST OF ACRONYMS

cps	counts per second
EI algorithm	Energetic Ion flux algorithm
FOV	field-of-view
GOES	Geostationary Operational Environmental Satellite
LEO	low Earth orbit
MeV	mega-electron volt
NaN	not a number
NPOESS	National Polar-orbiting Operational Environmental Satellite System
OMNI	omni-directional detector
POES	Polar Orbiting Environmental Satellite
SEISS	Space Environment In-Situ Suite (part of the SGPS on GOES-R)
SEM-2	Space Environment Monitor on POES
SEM-N	Space Environment Monitor for NPOESS (not built)
SEP	solar energetic particle (event)
SGPS	Solar and Galactic Proton Sensor
SWPC	Space Weather Prediction Center

1   INTRODUCTION

This document fully describes the algorithm theoretical basis plus supporting information for producing the differential particle fluxes for the omni-directional (OMNI) detectors in the Space Environmental Monitor (SEM-2) instrument package on the Polar Orbiting Environmental Satellite (POES) and MetOp satellites. The algorithm is referred to as the energetic ion flux (EI) algorithm. The following section provides a brief mission overview including general descriptions of the spacecraft bus, communications infrastructure and ground processing architecture, and the SEM-2 sensor suite hardware and software. Section 3 provides a scientific description of the algorithm required to process the SEM-2 OMNI data into differential number fluxes, including the mathematical description of the algorithm, processing procedures, identified sources of error, and algorithm inputs and outputs (I/O). Section 4 describes the test and proxy data sets used to validate the algorithm. Section 5 of this document consist of key assumptions and limitations, including software and hardware performance, references, and other pertinent information.

2 OBSERVING SYSTEM OVERVIEW

The SEM-2 OMNI instrument has been used on NOAA 15-19 (POES satellites) and has been/will fly on the MEPED A-C satellites. The POES and MetOp satellites are in Low Earth Orbiting (LEO) satellite with altitudes near 840 km, inclinations above 98°, and periods of about 102 minutes. The OMNI instrument characteristics and raw data structure are described in the document by Evans and Greer (2006). Launch dates for the various satellites carrying SEM-2 instruments are given in Table 1.

Table 1. POES and MetOp satellites which carry SEM-2 instruments as of April 2012. (From http://www.oso.noaa.gov/poesstatus/).

Satellite	Launch Date	Operational Date	Decommission Date	Morning/Afternoon Orbit
NOAA 15	13 May 1998	15 December 1998	--	AM
NOAA 16	21 September 2000	20 March 2001	--	PM
NOAA 17	24 June 2002	15 September 2002	--	AM
NOAA 18	20 may 2005	30 August 2005	--	PM
NOAA 19	6 February 2009	2 June 2009	--	PM
MetOp A	19 October 2006	21 May 2007	--	AM
MetOp B	23 May 2012 (planned)	--	--	--
MetOp C	2017 (planned)	--	--	--

In the SEM-2 package, the two lower energy detectors (P6 and P7) have 2-s integration times while the higher energy detectors (P8 and P9) have 4-s integration times. For this algorithm, the detectors are referred to as numbers 0 (lowest energy) to 3 (highest energy). Cross sections of the four omni-directional detectors in SEM-2 instrument package are shown in Figure 1. It can be seen that the higher energy detectors (on the left) have more shielding on the domes.
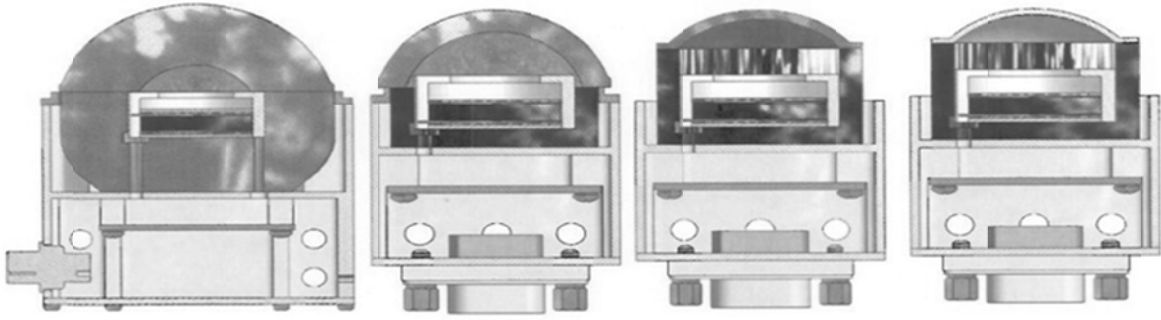
Figure 1. Cross sections of four omni-directional detectors in SEM-2 instrument package.

3 ALGORITHM DESCRIPTION

3.1 Algorithm Overview

The EI algorithm converts ion count rates (ions/sec) into differential flux spectra with units of ions / (cm^2 s sr MeV). The basic equation to be solved is to determine the differential proton flux $j(E, \theta, \varphi)$ from the count rate c_i for channel i:

$$c_i = dt\, \eta_i \int_0^A dA \int_0^\infty \int_0^{2\pi} \int_0^{\pi} j(E, \theta, \varphi)\ G_i(E)\ G_B(\alpha_B, \theta, \varphi)\ \sin\theta\, d\theta\, d\varphi\, dE + b$$

where b is the background count rate, dA is the area of the detector, dt is the duration of the measurement, E is the energy, $G_B(\alpha_B, \theta, \varphi)$ is the particle angular distribution function for the pitch angle α_B, $G_i(E)$ is the detector response including the field of view (FOV), and η_i represents the change in response due to detector aging,

The fundamental assumption of this algorithm is that over short energy ranges the differential directional energy spectrum of solar ions above 1 MeV follows a power law in kinetic energy, with an exponent that varies with energy. This assumption is well supported by observations of solar and magnetospheric ions with energies in the 100's of keV to MeV range [e.g., Baker et al., 1979; Lario and Decker, 2002].

The four omni-directional detectors provide the EI algorithm with 1-s proton count rates in four overlapping energy bands: 16-35, 35-250, 70-250, and 140-250 MeV. First, the algorithm redistributes the count rates into a new set of four non-overlapping energy channels. Then it iterates a piecewise power law fit over adjacent channels in order to derive a differential flux spectrum. The calculations include the energy-dependent geometric factor (response function + FOV) for each detector channel. The basis of this algorithm is the SEISS Integral Flux Algorithm for GOES-R [Rodriguez, 2009].

The primary algorithm outputs are four pairs of power law exponents and coefficients which define the derived differential flux spectrum over the entire energy range of the input channels. Also produced is the total flux in each of the five non-overlapping channels. The algorithm sets limits and defaults on the value of the power law exponents, γ, in order to avoid using unrealistically extreme or noise-sensitive values of this parameter. Since γ is solved iteratively, the algorithm places a limit on the number of iterations. Flags are set when defaults are used, limits are reached, or input data are missing.

3.2 The Particle Environment Measured by POES

The greatest proton fluxes above 10 MeV are observed during solar energetic particle (SEP) events. These energetic ions (as well as electrons and heavy ions) are believed to originate

in shocks and magnetic field reconnections associated with coronal mass ejections (CME) [Cane and Lario, 2006]. The measurement of proton fluxes in polar orbit has both operational and scientific applications. These fluxes are sufficiently energetic to impact satellites in the region, causing undesired transient responses and single-event upsets and permanent damage in solid state and solar cell devices [Baker, 1996]. Measurements of proton fluxes support alerts and warnings of radiation hazards to occupants of manned spacecraft and polar-crossing aircraft [Baker, 1996] and serve as inputs to operational predictions of D-region absorption of high-frequency and very-high-frequency (HF/VHF) radio waves [Sauer and Wilkinson, 2008] and to models to determine the polar cap boundary.

On its polar orbit, POES passes through several different regions of higher proton concentrations. Ions from SEP events are detected at high L-values (above about L>2.5) where they are directly injected into the polar regions during geomagnetic storms. The SEPs have a broad spectrum and are detected in all of the OMNI instruments. Following geomagnetic storms, new proton belts with energies in the 2-15 MeV range are sometimes created from ions injected at locations of about L=2 to 3.5 [Lorentzen, 2002]. A third set of energetic ions encountered by POES are those in the South Atlantic Anomaly (SAA). These trapped ions have energies covering all bands of the omni-directional detectors. In the SAA the ion fluxes are found mostly at L<1.6 and are not impacted by magnetic activity or SEP events [Evans, 2008].

Background counts on POES are due to galactic cosmic rays (GCRs) and are highest near the magnetic poles. The background count rates are below 1 cps. An example of a quiet period from POES data is shown in Figure 2a. An example of the high count rates detected during a SEP event is shown in Figure 2b.
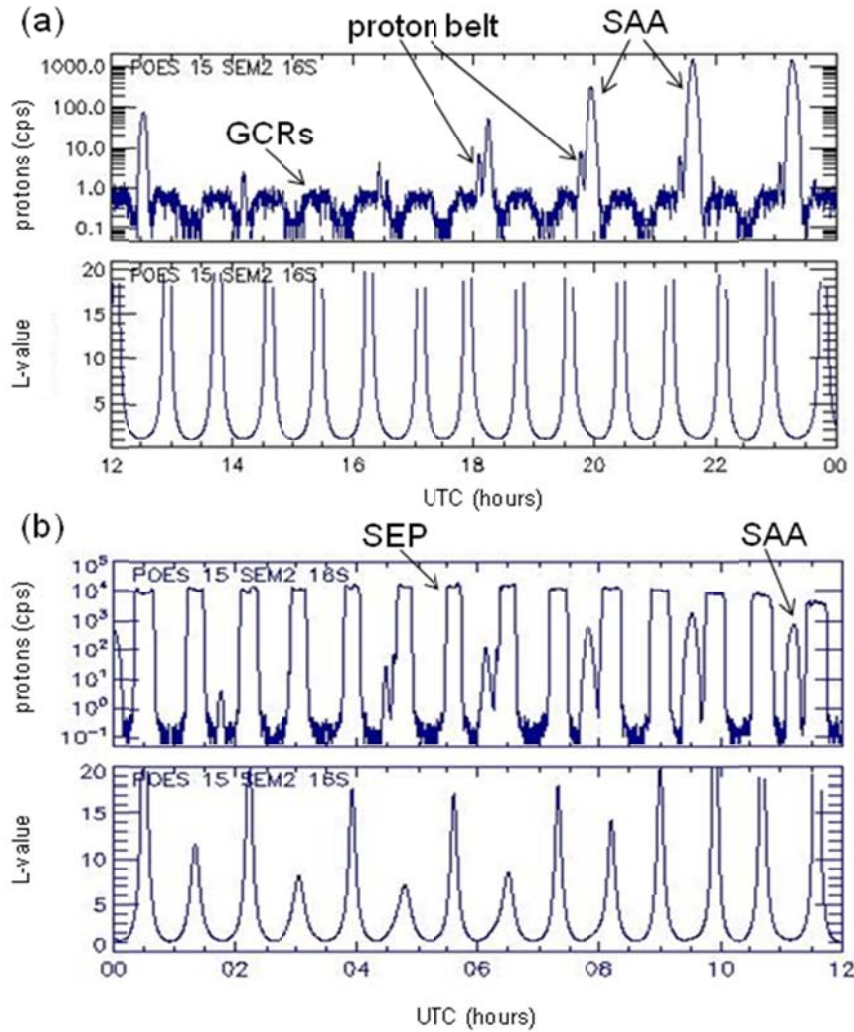
Figure 2. Proton counts in the lowest channel (≥16MeV) of the POES omni-directional detectors on NOAA-15 over six-hr periods. Also shown are the L-values at the satellite. (a) Data from a quiet period (1 January 2003) showing background counts due to GCRs as well as peaks from the SAA and a temporary proton radiation belt. (b) Data taken during a large geomagnetic storm (29 October 2003) showing the high count rates over the poles due to SEPs and the peaks dues to the SAA.

The calculation of the differential flux requires assumptions about its spectral shape. If a single statistical representation of the spectrum can adequately fit the data, that would simplify the calculation. For example, a monotonic decrease in flux with energy might be fit with a power law, $j(E) = j_0 E^\gamma$. In general, however, the spectrum of SEPs is not represented adequately by a single power law. The onset of a SEP event is a very important case (Figure 3), in which the highest energies arrive first (within tens of minutes of the acceleration of the source population to MeV energies). During such a period, when the

data clearly exhibit velocity dispersion, the exponent γ varies from positive to negative in a single energy spectrum. Therefore, since the differential flux spectra are sometimes not adequately represented by a single power law distribution, especially during times of interest, it is better not to base the calculation on this assumption. Instead the algorithm uses a piecewise fit of power law functions to the spectrum.
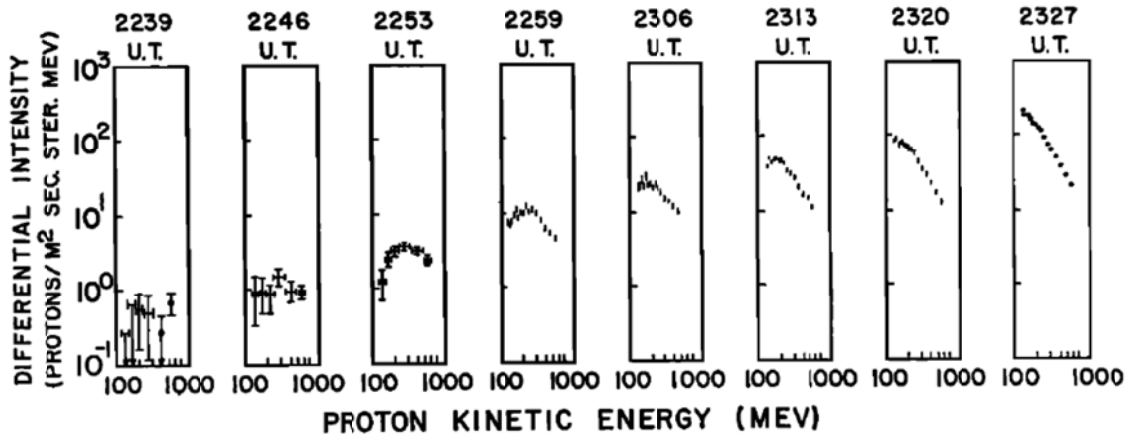
Figure 3. Rapid evolution of the 100-600 MeV spectrum of solar protons at 7-minute intervals during the onset of the SEP event of September 28, 1961, as measured by Explorer 12 [from Rodriguez, 2009; after Bryant et al., 1962, Figure 11].

The SEPs, which occur at high L-values, are assumed to have an isotropic pitch angle distribution. Trapped ions, which are detected at lower L-values, occur in a local pitch angle range (relative to the B field) between $90° - \propto_{max}$ and $90° + \propto_{max}$, where B_{sat} is the magnetic field at the satellite, and B_{120} is the magnetic field strength at an altitude of 120 km below which any particle is assumed to be lost to the atmosphere, and $\propto_{max} = sin^{-1} \sqrt{B_{sat} / B_{120}}$; the angles outside of this range are referred to as the loss cone [Evans, 2008]. The pitch angle distribution of the trapped particles is assumed to have the form $sin^n [(\alpha / \alpha_{max}) 90°]$ where n is frequently chosen to be 2, but near the equator may be much larger. The analysis in the EI algorithm does not currently include consideration of the overlap of the pitch angle distribution of particles. Other error sources not included in the algorithm include energetic neutral ions, satellite charging, and high energy electrons which are mis-counted as protons.

3.3 Mathematical Description

The EI algorithm determines the differential proton flux spectrum from the proton count rates produced by the SEM-2 omni-directional detectors. Challenges in this algorithm are that there are only four input channels, the channels overlap in energy, and there are energy-dependent correction factors.

The count rates are an integral of the differential flux and geometric factors. In order to estimate the integral of a function, a summing method can be used. The range is segmented into sub-ranges where the area under the curve can be well-represented by a simple function. These pieces of smaller area are then summed to provide the total integral. This estimation becomes better as the sub-ranges are made smaller.

The sub-ranges in these calculations are defined by the bandwidths of the detectors, and therefore cannot be made narrower to more accurately represent the differential flux spectrum. The proton measurements are made in channels that are rather wide in comparison to the energy dependence of the differential flux spectrum. Since the spectrum between the measurement values is not likely to be linear, we improve the estimation by applying an appropriate functional form to the curve between measurements. At these energies, a power law is a physically acceptable model of the differential flux spectrum that has been used extensively in legacy algorithms.

This procedure is based on the approach of the SEISS Integral Flux Algorithm for GOES-R [Rodriguez]. For the POES/MetOp EI algorithm, the particle count rates, C_i, are in adjacent channels with non-overlapping energy ranges. Center energies, E_i, are defined for each channel, i, and then power law fits of the differential flux,

$$j_i(E) = j_{0,i} E^{\gamma_i} \tag{1}$$

are made over the ranges between the center energies. The power law expression implicitly assumes that the energy is normalized to some reference energy such that $j_{0,i}$ is the flux at this energy and the term E^{γ_i} is a unitless function. For the solar proton integral fluxes, the natural reference energy is 1 MeV and the differential flux units are ions cm^{-2} s^{-1} sr^{-1} MeV^{-1}. Constraints are that the differential flux from adjacent fits must match at the center energies,

$$j_i(E_i) = j_{i+1}(E_i),$$

and that E_i is a midpoint (i.e., "center-of-mass") energy such that

$$C_i = G_i\, j_i(E_i)\, (E_u - E_l)\, dt.$$

where the G_i are the detector effective geometrical factors. A solution to these equations is found by iteratively calculating the channel center energy, E_i, and then the power law parameters, $j_{0,i}$ and γ_i, until the values of E_i converge.

Several modifications to the GOES-R procedure were required for use with the SEM-N data in the EI algorithm. First, the GOES-R technique assumes that the detectors have a constant response as a function of energy. The EI equations can maintain a similar form with the approximation that the detectors have piecewise power law responses. The GOES-R technique also requires that the detector channels should not overlap. For the EI algorithm, this requires converting the given overlapping channels into non-overlapping channels. This is done with some initial fit estimates using default values for the power law exponents.

The proton differential flux spectrum, $j_i(E)$, and the detector response, $g_i(E)$, are assumed to have power law forms in each region i:

$$g_i(E) = g_{0i}E^{\delta_i} \tag{2}$$

To simplify the following expressions we define:

$$\beta_i = \delta_i + \gamma_i \tag{4}$$

The associated count rate over region i is

$$C_i = \int_{E_l}^{E_u} g_{0i}E^{\delta_i} j_{0,i} E^{\gamma_i} \, dE \, dt \tag{5}$$

$$= \frac{g_{0i} j_{0,i}}{(\beta_i + 1)} \left(E_u^{\beta_{i+1}} - E_l^{\beta_{i+1}}\right) dt \tag{6}$$

where E_u and E_l are the upper and lower limits of energy range i. From Eq 6 we obtain an equation for the differential flux coefficient:

$$j_{0,i} = \frac{C_i\,(\beta_i+1)}{g_{0i}\,\left(E_u^{\beta_{i+1}} - E_l^{\beta_{i+1}}\right) dt} \tag{7}$$

Next we define an "uncalibrated flux", k, which is the detected differential flux without the geometric factors. This is given by

$$k_i = \frac{C_i}{(E_u - E_l)\, dt} \tag{8}$$

In region i, there is some midpoint energy E_i (Figure 4) such that

$$k_i = g_i j_i = g_{0i} j_{0,i} E_i{}^{\beta_i} \tag{9}$$

The initial guess for each E_i is the geometric mean in the energy range given by

$$E_i = \sqrt{E_u E_l} \tag{10}$$

To derive the power law fit, we take the ratio of the k_i and k_{i+1} at E_i noting that $j_i = j_{i+1}$ since the adjacent fits should match at this point.

$$\frac{k_{i+1}}{k_i} = \left[\frac{g_{0,i+1}\, j_{0,i}}{g_{0i}\, j_{0,i}}\right]\left[\frac{E_{i+1}{}^{\delta_{i+1}}}{E_i{}^{\delta_i}}\right]\left[\frac{E_{i+1}{}^{\gamma_i}}{E_i{}^{\gamma_i}}\right] \tag{11}$$

Given that $a^x = e^{x \log a}$ and $\log a - \log b = \log\frac{a}{b}$, we find

$$\frac{k_{i+1}}{k_i} = \left[\frac{g_{0,i+1}\, E_{i+1}{}^{\delta_{i+1}}}{g_{0i}\, E_i{}^{\delta_i}}\right]\left[\frac{e^{\gamma_i \log E_{i+1}}}{e^{\gamma_i \log E_i}}\right]$$

$$= \left[\frac{g_{0,i+1}\, E_{i+1}{}^{\delta_{i+1}}}{g_{0i}\, E_i{}^{\delta_i}}\right] e^{\gamma_i \log(E_{i+1}/E_i)}$$

The power law exponent for this region is then

$$\gamma_i = \frac{\log[\, g_{0i}\, E_i{}^{\delta_i}\, k_{i+1}/\, g_{0,i+1}\, E_{i+1}{}^{\delta_{i+1}}\, k_i]}{\log(E_{i+1}/E_i)} \tag{12}$$

Given γ_i (and hence β_i), we can now find the new E_i for this iteration. Reordering Eq. 9 and substituting from Eqs 8, we get

$$E_i{}^{\beta_i} = \frac{C_i}{g_{0i} j_{0,i}\, (E_u - E_l)\, dt} \tag{13}$$

Substituting for C_i from Eq 6 yields

$$E_i{}^{\beta_i} = \frac{E_u{}^{\beta_i+1} - E_l{}^{\beta_i+1}}{(\beta_i + 1)\,(E_u - E_l)} \tag{14}$$

$$E_i = \left[\frac{E_u{}^{\beta_i+1} - E_l{}^{\beta_i+1}}{(\beta_i + 1)\,(E_u - E_l)}\right]^{1/\beta_i} \tag{15}$$

Then, the power law coefficient determined from Eq 9 is

$$j_{0,i} = \frac{k_i}{g_{0i}}\, E_i{}^{-\beta_i} \tag{16}$$

In practice, the calculations of γ_i and then E_i and j_{0i} are iterated until the change in E_i is adequately small. The integrated flux can be calculated with the final values of γ_i, E_i and j_{0i} is

$$J_i = \int_{E_i}^{E_{i+1}} j_{0,i} \, E^{\beta_i} \, dE \tag{17}$$

$$= \frac{j_{0,i}}{\beta_i+1} \left(E_{i+1}^{\beta_i+1} - E_i^{\beta_i+1} \right) \tag{18}$$

3.1.1 Simple Fit

As described in the next section, for cases where there the count rate is low, a simple fit to the data is made with a single power law using count rates in the lowest two non-overlapping channels. A "two point" fit is preferred, but if that cannot be made, then a "one point" fit is made.

The fit of two channels to a single power law is done as follows at E_0 and E_1. First, using a^x = exp(x log a), Eq. 1 expands to

$$j(E) = j_0 E^\gamma = j_0 \, e^{\gamma \ln E} \tag{19}$$

Here the subscripts have been removed, since there will be only one power law fit for all ranges. A linear expression is created by taking the logarithm of both sides of Eq. 19 to produce

$$\ln[j(E)] = \ln j_0 + \gamma \ln E \tag{20}$$

For two midpoint energies, E_0 and E_1 and with an estimate of the flux at each of the energies, the power law parameters of j_0 and γ are then

$$\gamma = \frac{\ln[j(E_0)/j(E_1)]}{\ln[E_0/E_1]} \quad \text{and} \tag{21}$$

$$j_0 = j(E)/E^\gamma \tag{22}$$

For a single point fit, for the energy, E_i, the flux parameters are

$$\gamma = \gamma_{default} \quad \text{and} \tag{23}$$

$$j_0 = j(E_i)/E_i{}^{\gamma_{default}} \tag{24}$$

In this case, the j_0 used is the average of that calculated at E_0 and E_1.
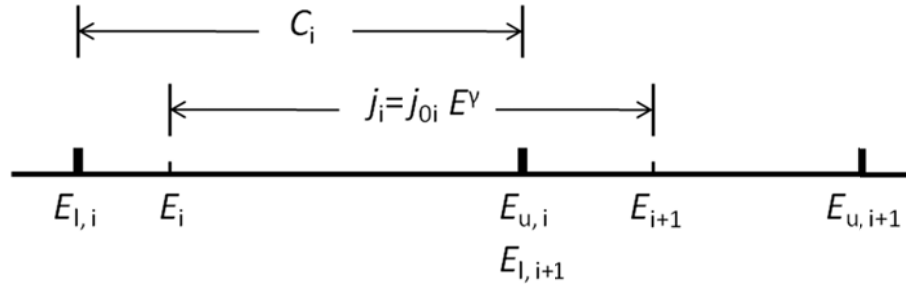
Figure 4. The relative locations of some variables including several upper and lower channel edges (E_u and E_l) and the midpoint energies (E_i). Note that the ranges for channel count rates (C_i), and the differential flux (j_i) are offset since the differential flux fits are calculated between the midpoint energies.

3.4 Processing Procedure

A summary of the steps in the algorithm follows. The original data in overlapping channels is referred to as "raw count rates" and "raw data channels", while that in the EI-algorithm-generated non-overlapping channels are referred to as just "count rates" and "channels". No background subtraction is performed because the background count rates are <1 cps (Figure 2).

1. Read in raw proton count rates in overlapping energy channels from the four omni-directional detectors. If any of these values are negative or NAN, then all output will be set to -999.
2. Generate initial estimates the differential flux spectrum using a default power law exponent, $\gamma_{default}$. (Eq 7)
3. Convert raw count rates to count rates in four non-overlapping energy channels using the initial differential flux spectrum. If the sum of raw count rates < 25, if any of the new count rates are negative, or if the sum of the count rates in the the first three channels is <1, skip Steps 4 and 5 and do the simple fit routine in Step 6.
4. Initialize E_i with the geometric mean of the channel edge energies. (Eq 10) These initial values do not impact the solution.
5. *Full fit routine:* Iterate to determine power law parameters, $j_{0,i}$ and γ_i.
   a. Estimate the set of γ_i using the set of E_i. (Eq 12) If any $|\gamma_i|>8$ or if the slope in the highest energy leg is positive ($|\gamma_2|>0$), then skip to the simple fit routine (Step 6).
   b. Estimate a new set of E_i using the new set of γ_i. (Eq 15)

c. Since there are two E_i's associated with each channel (except for the lowest and highest energy channels), one below the center energy and one above the center energy, there are two new E_i's for each channel. Linearly average the two estimates to derive the new estimate of E_i going forward.

d. Compare new E_i with previous E_i. Reiterate Steps 5a-d until the convergence criterion that all channels are changing by < 1% is met. If, after ten iterations, the value of E_i is still changing by more than 1%, then stop the iteration and do the simple fit routine in Step 6.

e. Calculate the set of $j_{0,I}$ from the final set of E_i and γ_i. (Eq. 16)

f. Extrapolate from the adjacent fits to cover both ends of the range of the channels; i.e., select γ_0 and $j_{0,0}$ for $E_{l,0}$ to E_0, and γ_4 and $j_{0,4}$ for E_4 to $E_{u,4}$.

6. *Simple Fit Routine*: If there were errors in converting from raw count rates or during the iteration, generate a single power law fit to the entire differential flux spectrum using the count rates for channels 0 and 1. For either type of simple fit (one-point or two-point) the resulting $\gamma < 0$. Before starting the calculations, if $cn[ii]<0$ for ii=0 or 1, that $cn[ii]$ is set to 0.

a. Estimate $j(E_0)$ and $j(E_1)$ for the lowest two channels. (Eqs 8 and 9)

b. If $C_0>0.01$, $C_1>0.01$, and $j(E_0)>2* j(E_1)$, and then do a
Two-point fit: use $j(E_0)$ and $j(E_1)$ to define a single power law fit over all channels (Eqs 21 and 22).

c. If didn't do a two-point fit or the two-point fit produced $\gamma< -8$, then do a
One-point fit: If either $j(E_0)$ or $j(E_1)$ is <0.00001 it is reset to 0.0001
Determine the coeficients, γ_0 and γ_1, at both E_0 and E_1 using Eq. 24. The final parameters for the single power law fit over all channels are the default power law exponent, $\gamma_{default}$, and the average of $j_0(E_0)$ and $j_0(E_1)$.

7. Calculate differential flux at desired energies to output. (Eq. 1)

8. Calculate estimated errors on differential flux (Section 4.5).

9. Set exception handling flags as needed.

In general, the non-simple fit requires only two or three iterations to converge. Setting the convergence threshold to 0.1% or less has a negligible effect on the results and increases the number of iterations by at most one.

A default power law exponent, $\gamma_{default}$, is used at several points in the algorithm. The value of -2.9 was obtained by temporarily setting all of the fits to simple fits and finding the average γ for 2-pt fits of NOAA-15 data for the year of 2003.

Differential flux is calculated in two ways and over two different sets of regions. Rough initial estimates are given over the channel ranges using Eq. 6 and $\gamma_{default}$. The iterative fit routine which determines γ_i and $j_{0,i}$ is applied to the ranges between the midpoint energies.

The conversion from the raw count rates of the omni-directional detectors, O_i, to count rates in non-overlapping channels, C_i, requires several steps. The elements of this conversion are portrayed in Figure 5. The subtraction of count rates from the various channels must be done in piecewise fashion because the functions for the geometric factors are defined piecewise in energy. Calculations are started from the highest energy channel. Since both channels cover the same range from 140 to 250 MeV, $C_3 = O_3$.

The next step is to determine C_2. First an estimate of differential flux function j_3 over the range 140 to 250 MeV is made using Eq. 7, the relevant geometric factors for channel 3, and $\gamma_{default}$. Next, the count rate in this range on detector 2, $C_{2,j3,140\text{-}250\text{ MeV}}$, are found using j_3 and the relevant geometric factor for channel 2, g_2. Then $C_2 = O_2 - c_{2,j3,140\text{-}250\text{ MeV}}$. From C_2 an estimate of j_2 is made.

The count rates on the lower three energy channels are found in a similar fashion. Because the geometric factor ranges do not overlap perfectly for channel 1, multiple terms are needed to calculate the count rate there: $C_1 = O_1 - C_{1,j3,140\text{-}250\text{ MeV}} - C_{1,j2,90\text{-}140\text{ MeV}} - C_{1,j2,\ 70\text{-}90\text{ MeV}}$. From C_1 an estimate of j_1 is made. Similarly, the count rate for the lowest energy channel is given by $C_0 = O_0 - C_{0,j2,90\text{-}140\text{ MeV}} - C_{0,j2,\ 70\text{-}90\text{ MeV}} - C_{0,j1,\ 35\text{-}70\text{ MeV}}$.
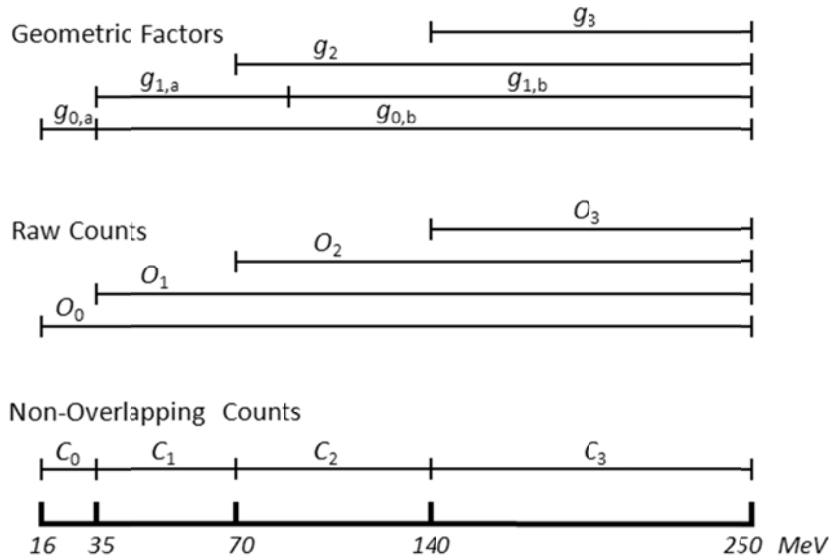
Figure 5. The overlapping energy ranges of the raw count rates from the omni-directional detectors, O_i, and the derived non-overlapping ranges for the final count rates, C_i. Also shown are the non-zero FOV and geometric factors.

The simple fit routine is used when some of the converted count rates are negative or very small. This occurs when the particle fluxes in some of the energy channels are near background levels. During these times when the measurements may be in the noise level, the calculation of γ_i and j_0 can be greatly affected by small variations in the background count, and not representative of the actual population. The simple fit routine is also used when the power law fits produce very large exponents; this occurs when some channels (generally lower energy ones) have very high count rates, but adjacent channels are near background levels. The threshold for using the simple fit routine is when the sum of the four detector count rates is <25. For the simple fit routine, the algorithm disregards the higher energy channels and uses just the first two channels to set a single power law fit across the entire range.

A cartoon of the technique is show in Figure 6. The three power law fits between the E_i are shown as well as the extrapolations to the edges of the detector ranges. Slope discontinuities occur at the E_i.
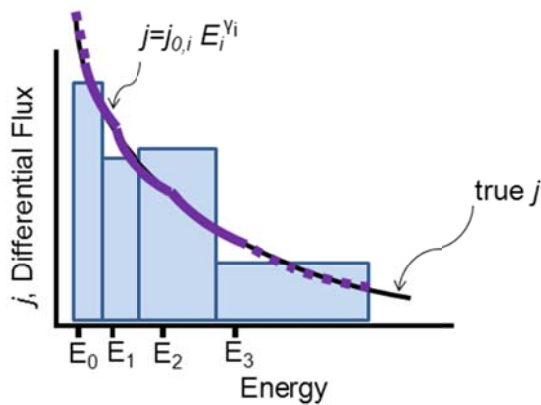
Figure 6. Cartoon of technique. Power laws are calculated between E_i (solid purple lines) and extrapolated to edge of energy range (dashed purple lines). The true differential flux is also shown (black line). The count rates, C_i, for the four detectors are represented by the blue boxes.

3.5 Algorithm Input and Output

The input to the algorithm consists of the count rates from the four SEM-2 omni-directional detectors, and ancillary data describing the response functions of the individual detectors.

3.5.1 Primary Sensor Data

The differential flux calculation uses the four channels of the OMNI proton count rates. The sampling times are 2 s for the two lower energy detectors and 4 s for the two higher

detectors. The accumulation times end 0.2 s after time stamps according to Evans and Greer [2000].

In specifying the FOV center direction relative to the ENP coordinate system, it is assumed that the spacecraft axes are aligned to this coordinate system (where N is the normal to the orbital plane and E is directed toward the Earth along this plane). Given the large FOVs, this is not a critical assumption for small (~1 deg) differences between the spacecraft and ENP axes. The omni-directional detectors are mounted on the spacecraft with the central axis of the dome directed off-axis to E and along P by 9° [Evans and Greer, 2000].

Table 2. SEM-2 OMNI 1-s inputs to EI algorithm.

Quantity	Number of Values	Units	Purpose in Calculations
Proton count rates	4	cps	Basis for flux calculations

3.5.2 Auxiliary Data

No auxiliary data is needed by the algorithm.

3.5.3 Ancillary Data

Ancillary data are data that are not generated by SEM-2 or the spacecraft on-orbit or by the ground processing system. The ancillary data required by the EI algorithm include of characteristics of the OMNI channels (Table 3). These characteristics consist of their response functions (i.e., geometrical factors) as a function of energy. These data are products of the characterization of the HES in ground test and analysis. The geometrical factors are fit with power laws as a function of energy for ease of use in the EI algorithm. For some detectors, with a flat response at low energy, there are power laws fits for two energy ranges.

Table 3. Ancillary data related to OMNI performance characteristics required by the EI algorithm.

Quantity	Refresh	Number of Values	Units	Purpose in Calculations	Source
Energy boundaries of detector response function	Static	3 energy boundaries (representing 2 energy ranges)	MeV	To calculate band centers and average fluxes	Ground calibration

Quantity	Refresh	Number of Values	Units	Purpose in Calculations	Source
Detector response functions	Static	Power law response functions (1 exponents and 1 coefficients) on one or two energy ranges for each of the detector. In software version 1.0 there are a total of 6 functions for the four detectors.	cm^2 sr	To calculate average fluxes	Ground calibration
Software version number	Static	Two integers (i, j). Version number is of the form "i.j"	none	May define changes to other static values.	Software
Output energy values	Static	For software Version 1.0, there are 3 energies: 25, 50 and 100 MeV.	none	Energies at which to calculate output average fluxes	Software

3.5.4 Algorithm Output

The EI algorithm creates power law fits to the differential proton flux spectrum. The fits are made to three adjacent energy intervals which fully cover the energy range of the four input channels. The coefficients, exponents and energy ranges of the fits are output. Other output values include the differential flux at three specific energies chosen to be near the geometric means of the channel energies, the fractional error on the flux and quality flags. The data outputs are shown in Table 4 and flag outputs are shown in Table 5. The non-integer output values are converted to float data types from doubles to save file space.

Table 4. Data output from EI Algorithm.

Name	Description	Data Type	Number of values	Units
Eedge1	Boundaries of energy ranges for power law fits to differential proton flux	float	4	MeV

jf0	Coefficients of power law fits to differential proton flux	float	3	ions / (cm^2 s sr MeV)
gamma0	Exponents of power law fits to differential proton flux	float	3	none
j_out	Differential proton fluxes at 25, 50 and 100 MeV	float	3	ions / (cm^2 s sr MeV)
fract_err	Average fractional error on fluxes	float	1	none
[flags]	Error/quality flags (see Table 5)	int	6	see Table 5
version	EI software version number	int	2	none

Table 5. Flags output by EI algorithm. All flags are integers. Values are 1=true, 0=false unless otherwise stated.

Flag	Cause	Result
bad_cn	Non-overlapping channel count rates are 'NaN'. Note: this seldom if ever occurs.	Record is not processed.
bad_omni_cts	OMNI count rates are negative or 'NaN'.	Record is not processed.
fit	-1= No fit performed. 0= Power law fit with different γ and j_0 over four regions 1 = simple "one point" fit: Fit all energies with a single γ and j_0 based on count rates in first two channels and $\gamma = \gamma_{default}$. 2 = simple "two point" fit: Fit all energies with a single γ and j_0 based on count rates in first two channels.	Defines fit used.
gamma_lim	For some i, $|\gamma_i| > 8$.	Use a fit with a single γ and j_0.
highE_slope_pos	Initial fit produced slope>0 ($\gamma_2 > 0$) for highest energy range	Use a fit with a single γ and j_0.

Flag	Cause	Result
iter_lim	For some $i,$, exceeded number of allowed iterations (10) to determine E_i.	Use a fit with a single γ and j_0.

4   TEST DATASETS AND ERROR BUDGET

The proxy data for the OMNI detectors is discussed in Sections 4.1 through 4.3. The sources of error for this algorithm and the error calculations are discussed in Section 4.4.

4.1 Simulated/Proxy Input Data Sets

The proton differential flux calculation requires input of proton count rates in four channels. Proxy count data are created from several sources and are intended to represent a wide range of conditions for the OMNI detectors. The test data sets include a mix of quiet and active times and include occurrences of solar energetic particle (SEP) events. Proxy data include some extreme values and bad data points that can be used to exercise the algorithm. The software was set up to generate proxy data with either a prescribed spectral function or from POES 16-s averaged data.

To evaluate the errors due to the algorithm, the proxy data count rates must be generated from a "true" spectrum, and then the output of the algorithm compared with this "truth". This type of proxy data is created by (1) generating "true" differential energy spectra from real count data, and then (2) generating proxy SEM-N count rates based on these "true" spectra. The first step requires assumptions regarding spectral shape. The chosen spectral shape does not need to match reality perfectly in order for the generated spectra and associated proxy count rates to be good tests of the algorithm. Poisson noise can be added to the count rates to assess its impact on the algorithm as discussed in Sections 4.4 and 4.5.

4.2 Proxy data from POES measurements

Simulation software was set up to generate proxy data over any time range from 16-s averaged POES or MetOp OMNI data. The data was accessed from the NOAA NGDC archives and generally the NOAA-15 data was used to create the proxy values. The lowest channel of the POES omni-directional detectors is known to be contaminated by electrons, but this is not considered in the creation of the proxy data.

The EI algorithm is run using the proxy POES raw count rates and differential flux spectra are generated for the entire energy range of the detectors. These spectra are not used as "truth" because they have unrealistic discontinuities in slope at the center energies. Instead, the "true" spectrum is created by fitting the differential flux values, j_i at each of the center energies, E_i with a pair of overlapping power law functions. The lower energy fit is over j_0, j_1, and j_2, and the higher energy fit is over j_1, j_2, and j_3. The fit is accomplished by doing a linear fit to $\ln j$. The final spectrum is an interpolation of the two fits in the overlapping region between E_1 and E_2. Then, proxy detector count rates due to the "true" spectra are calculated assuming response functions of the OMNI detectors. The proxy

count rates are run through the algorithm and the differential energy flux spectrum output by the algorithm is compared to the "true" spectrum.

Table 6. POES omni-directional data channels.

algorithm channel number	POES channel	POES channel energy range (MeV)
0	P6	16-250
1	P7	35-250
2	P8	70-250
3	P9	140-250

Proxy data sets using POES data can be chosen to encompass SEP events including their onset, peak, and decay, and the magnetospheric-only populations preceding or following them such as the events that occurred over 10 days during the 2003 Halloween storm.

4.3 Proxy data from 2003 SEP fluence spectra studied by Mewaldt

The algorithm was also tested on data for the SEP events of October-November, 2003. Mewaldt et al. generated fluence spectra for five events during this time period using double power law fits:

$$dJ/dE = CE^{\gamma}\exp(-E/E_0) \quad \text{for} \ E \leq (\delta - \gamma)E_0;$$

$$dJ/dE = CE^{\delta}\{[(\delta - \gamma)E_0]^{\delta - \gamma} \, exp(\gamma - \delta) \ \text{for} \ E \geq (\delta - \gamma)E_0$$

The spectral functions defined by Mewaldt et al. were used to generate proxy count rates which were then processed by the EI algorithm. A comparison of the original spectra and the EI algorithm output are shown in Figure 7. For all points shown for the five cases, the average magnitude of the error was 2.4% with a standard deviation of 4%. There is no noise on this data, so it is a test of how well the algorithm fits the fluence spectral shape.
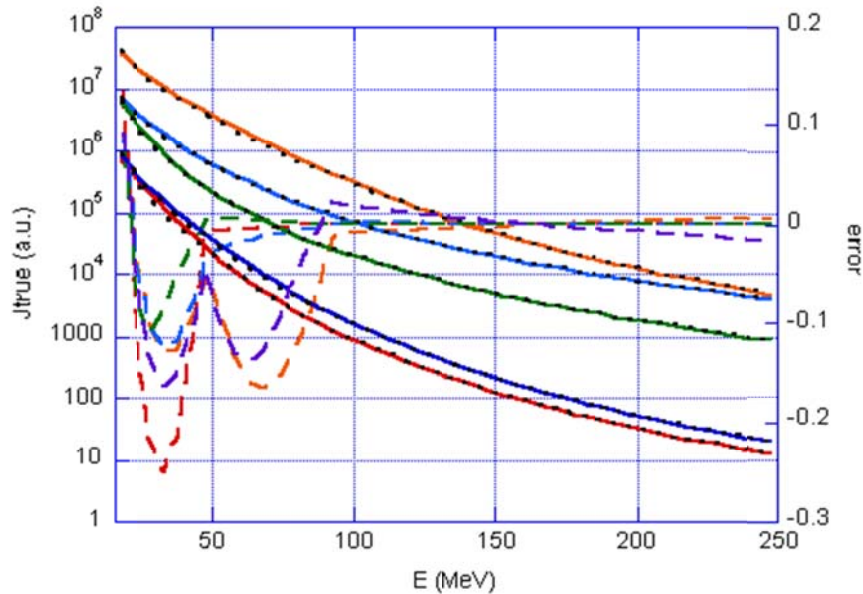
Figure 7. Comparison of power law fits to proton fluence spectra for five SEP events during October-November 2003 given in Table 5 of paper by Mewaldt (2005). The dots are the spectral shapes generated from the equations from Mewaldt et al., and the solid lines are the power law fits to those spectra produced by the EI algorithm. The average standard deviation for the derived spectra from the original spectra is 5%.

4.4 Error Determination

There are a number of sources of error that contribute to uncertainties in the EI EDR outputs. Factors include uncertainties in instrument correction factors, low spectral and angular resolution, overlap of downward loss cone with detectors, Poisson noise on the count data, and algorithm error.

The net algorithm plus instrument error is determined in two steps. First, the error budgets for the count rates for each channel are calculated. Then, this error is propagated through the algorithm with proxy data to obtain the statistics on how it impacts the output fluxes.
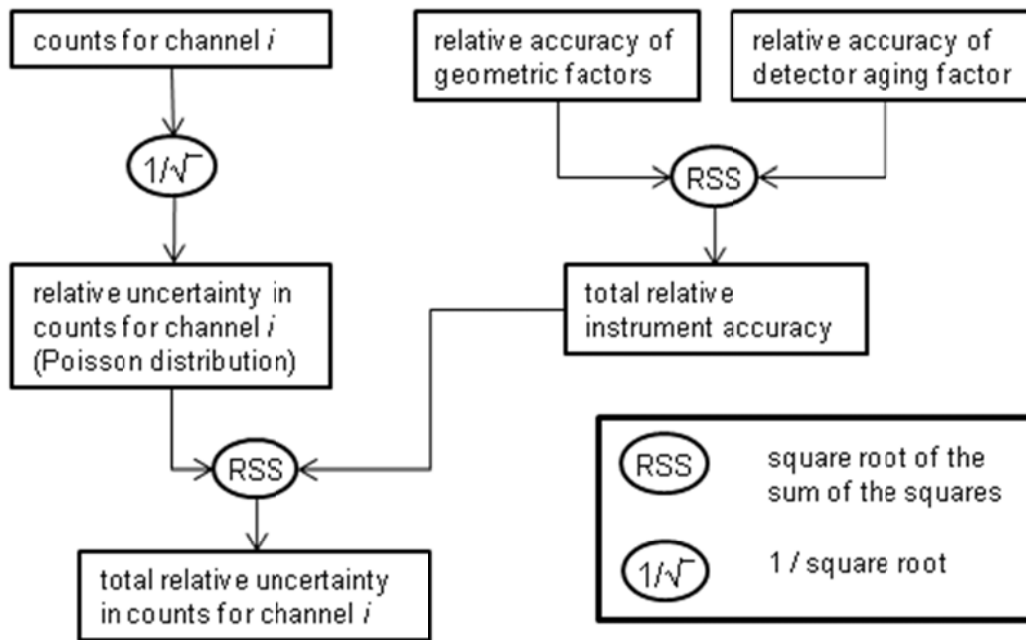
Figure 8. Error propagation for the count rates in one channel.

Figure 8 shows the error propagation of the main sources of errors for the count rates in one channel. Here, the root sum of the squares of independent relative uncertainties (RSS) is

given by $\dfrac{\sigma_z}{z} = \sqrt{\left(\dfrac{\sigma_x}{x}\right)^2 + \left(\dfrac{\sigma_y}{y}\right)^2}$. (25)

4.5 Error Estimates

As discussed in Section 4.1, for tests, "true" spectra are generated from the POES count rates and then proxy count rates are generated from these "true" spectra. An example fit is shown in Figure 9.
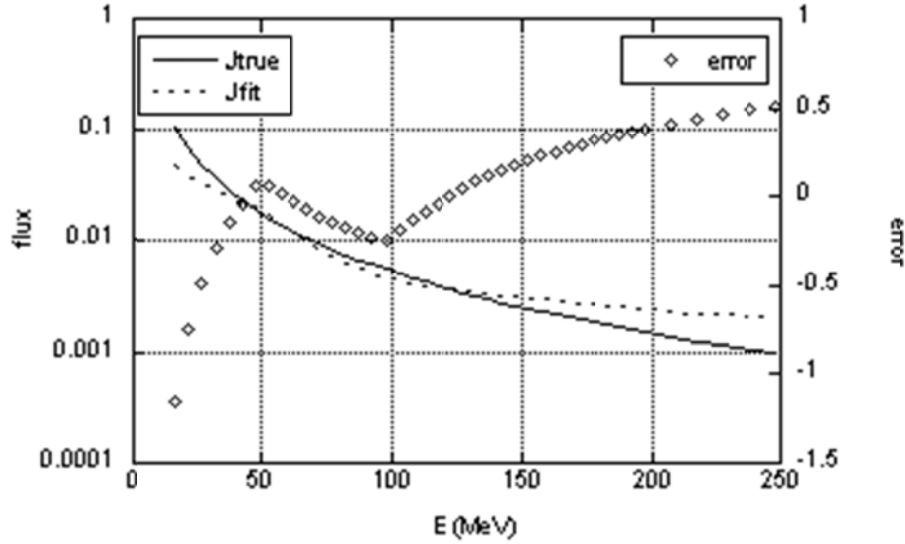
Figure 9.   Comparison of typical fit of flux (dotted line) to the "true" flux (solid line). Errors are shown with diamonds.

To determine the error statistics, Poisson noise was added to the proxy count rates and the output spectra were compared with the "true" spectra. We examined the standard deviations in a little more detail, by breaking up the output into three energy bands: 16-50 MeV, 50-100 MeV, and >100 MeV. We looked at the standard deviations in each of these bands as a function of the count rates in both the lowest energy channel and the sum of all of the channels to see how the standard deviations changed with low and high count rates. Of course, due to Poisson noise, we expect the largest deviations at the lowest count rates. We used these results to set the thresholds for when the simple fit should be applied.

Based on the values in Table 7, we choose a threshold for the fit routine of

$\Sigma omni[i] > 25$

where *omni*[*i*] are the count rates of detector channel *i* and $\Sigma omni[i]$ is over all 4 channels. Above this threshold are average standard deviations in the three energy ranges of 0.36, 0.27, and 0.38 and an overall average standard deviation of 0.36 (last line of Table 7). Considering that we are only looking at certain spectral shapes, this is probably a conservative estimate of the errors.

Table 8 shows the fractional error as a function of the detector count rates that is output by the algorithm. Where the error is based on the sum of the detector count rates ($\Sigma omni[i]$), the values come from the marked values in Table 7. For the simple fit case, we do not attempt to calculate errors, but rather set this error to 1.0 (100%). The error output by the algorithm (final column of Table 8) includes an additional error due to an estimated 20% error in the knowledge of the effective geometric factor (Section 6.1) which is added as a

root sum of the squares (Eq 25). This is a conservative estimate of the error. Other unquantified sources of error include the assumed spectral shape that we used for the proxy data and the assumption that the particle angular distribution is isotropic.

Table 7. Standard deviations (fractional error) of flux for three energy bands for the NOAA 15 satellite. Other thresholds were set to minimal values. Here Σomni= *omni*[0]+*omni*[1]+*omni*[2]+*omni*[3], where the *omni*[] are the original channel count rates.

date(s)	threshold	avg sd for *j* in 16-50 MeV	avg sd for *j* in 50-100 MeV	avg sd for *j* in >100 MeV	avg sd for *j* over full range	no. of values in avg	used to define output error
2003-05	15<Σomni<25	2.77	0.44	0.52	1.17	3800	
2003-05	25<Σomni<35	1.52	0.41	0.54	0.75	4100	
2003	25<Σomni<100	1.28	0.40	0.51	0.67	9500	
''	25<Σomni<50	1.44	0.42	0.56	0.74	3300	x
''	50<Σomni<100	1.19	0.39	0.48	0.62	6000	x
''	100<Σomni<250	0.75	0.33	0.38	0.45	11000	x
''	250<Σomni<500	0.51	0.26	0.31	0.34	10000	x
''	500< Σ omni<1000	0.42	0.22	0.27	0.29	12000	x
''	1000<Σ omni<5000	0.46	0.19	0.12	0.22	33000	
''	Σ omni>5000	0.38	0.24	0.22	0.25	2000	
''	Σ omni>1000	0.46	0.19	0.12	0.22	35000	x
''	Σ omni>25	0.66	0.26	0.29	0.37	78000	
Oct 2003	Σ omni>25	0.50	0.26	0.36	0.37	11400	
2000-09	Σ omni>25	0.72	0.26	0.28	0.37	850000	

Table 8. Error values output by the EI algorithm.

simple fit	range for Σomni	fractional error based on Poisson error only (from Table 7)	fractional error output by algorithm (includes 20% error on detector response)
no	25<Σomni<50	0.74	0.77
	50<Σomni<100	0.62	0.65
''	100<Σomni<250	0.45	0.49
''	250<Σomni<500	0.34	0.39
''	500< Σ omni<1000	0.29	0.35

| '' | Σ omni>1000 | 0.22 | 0.29 |
| yes | any, but generally Σomni<25 | 1.0 | 1.02 |

For proxy data created from the POES data, output statistics are shown in Table 9. The values were determined with a threshold for non-simple fits set to Σomni[i] >25 and Poisson noise added to the detector count rates.

Table 9. Statistics and other values for output spectra with added Poisson noise.

year(s)	key values		for proxy		fractions of data			statistics		
date(s)	avg sd for j	avg γ for 2-pt fit	avg γ_1 for proxy	avg γ_2 for proxy	fraction simple 1-pt fit	fraction simple 2-pt fit	fraction non-simple	fraction good pts	total recs	
2000-09	0.37	-2.7	-0.3	-1.7	0.66	0.30	0.04	0.999	1.9e7	
2000	0.39	-2.7	-0.3	-1.7	0.68	0.28	0.04	0.998	2.0e6	
2002	0.37	-2.8	-0.2	-1.6	0.67	0.29	0.04	0.999	2.0e6	
2003	0.37	-2.9	-0.3	-1.7	0.67	0.29	0.04	0.999	2.0e6	
2009	0.32	-2.5	-0.1	-1.7	0.65	0.30	0.05	0.999	2.0e6	
Oct 2003	0.37	-2.9	-1.2	-2.3	0.64	0.29	0.07	0.999	1.7e5	
29 Oct 03	0.40	-2.8	-2.7	-3.5	0.44	0.14	0.42	0.999	5396	
29 Oct-6 Nov 03	0.46	-3.1	-2.4	-2.8	0.48	0.36	0.17	0.999	4.8e4	

4.6 Other Tests

A simple test was performed to compare the outputs of this algorithm with the simple directional flux estimates given as J6-J9 in Appendix F of Evans and Greer (2006) for the POES OMNI detectors. These fluxes are calculated for energy ranges 16-35, 35-70, 70-140, and 140-500 MeV. Directional fluxes were calculated for the same ranges from the fits given by this algorithm (Table 10). This comparison verifies that the magnitudes of the algorithm output are reasonable. It also shows that some refinement is needed for the very simple Evans and Greer (2006) algorithm because it sometimes produces negative fluxes.

Table 10. **Six examples of comparisons of fluxes output by algorithm with fluxes from simple calculations of Evans and Greer (2006).**

trial #	channel	count rate	Evans flux	flux from algorithm fit
1	0	29	3	11
	1	25	-8	4
	2	34	3	13
	3	16	3	10
2	0	213	15	23
	1	195	27	64
	2	163	6	67
	3	130	24	82
3	0	1576	841	892
	1	586	199	336
	2	352	49	161
	3	81	15	46
4	0	3134	1483	1187
	1	1387	347	716
	2	978	160	403
	3	99	18	53
5	0	13039	8729	9708
	1	2757	1330	1895
	2	1190	205	493
	3	66	12	34
6	0	15856	11332	13130
	1	2508	1357	1832
	2	910	157	382
	3	47	9	24

5   PRACTICAL CONSIDERATIONS

5.1 Numerical Computation Considerations

The algorithm is straightforward to implement in software. The retrievals do not require matrix inversions. The most complex part of the algorithm, the iterative solution for the channel center energies and gammas, is limited in the number of iterations that can take place and generally requires less than three iterations. Although the measurements are single precision, the calculations takes advantage of the double precision capabilities of the host machine.

5.2 Programming and Procedural Considerations

The operational algorithm has been implemented in C. It uses many subroutines in order to maintain the readability and modularity of the code. The algorithm was originally developed for the proposed NPOESS SEM-N HES instrument and the software retains some variables to permit the 5-channel structure of the HES.

5.3 Quality Assessment and Diagnostics

Quality assessment of the operational product is based on the flags described in the next section. If error flags are set frequently, then either the instrument is having problems or there is a problem upstream in the data processing system. The single power law fits will be used frequently outside of SEP events.   The gamma limits should be invoked less frequently, primarily in temporary radiation belts. Based on testing with the proxy data, the energy iteration limit should be reached very infrequently.

5.4 Exception Handling

Instrument error handling is performed prior to this algorithm. Instrument errors or bad data are flagged by setting the detector count rates to -999. This algorithm requires a complete set (4 channels) of count rates to accurately determine the differential flux spectrum. Checks on the validity of the input, based on bad data flags threshold levels for the input are made by this algorithm. The flags are listed in Table 5.

In the presence of one or more missing differential flux values (assumed to be indicated by fill value such as -999.0 or NaN), the algorithm will not calculate the integral flux. Instead, it sets *flag_fit* to -1, most output values to -999, and any relevant flags to 1. In principle, it is possible to interpolate or extrapolate over a missing flux value. However, there are many possible permutations of missing flux values, and each could require a different algorithm. If the problem is random and infrequent, then it is not worthwhile to develop an algorithm to handle the problem. Should one or more channels in the OMNI fail for a particular satellite, then it may be possible to develop an algorithm to handle the specific situation.

5.5 Algorithm Validation

Differential flux measurements could also be compared with those made by the GOES-R instruments as POES or MetOp satellites pass by at much lower altitude. In this case, the differential flux from regions with the same L-value should be compared and the GOES data will need to be converted from integral flux to differential flux.

5.6 Performance

An important performance parameter is continuity of integral flux levels between satellites. Satellite-satellite intercomparisons are needed to ensure continuity of the operational product. Such intercomparisons could be made regarding count rates between various POES and MetOp satellites.

5.7 Assumed Sensor Performance

Table 11 lists expected instrument measurement performance for the SEM-2 on the POES and MetOp satellites.

Table 11. Expected measurement performance of the energetic ion detectors according to the SEM-2 specification.

Attribute	Threshold Performance
Measurement Ranges	
Proton Flux, E < 100 MeV	$5x10^3$-$2x10^9$ m^{-2} s^{-1} sr^{-1}
Proton Flux, E > 100 MeV	$5x10^3$-$2x10^9$ m^{-2} s^{-1} sr^{-1}
Measurement Resolution	
Proton Flux, E < 100 MeV	The greater of $5X10^3$ m^{-2} s^{-1} sr^{-1} or 10%
Proton Flux, E > 100 MeV	The greater of $5X10^3$ m^{-2} s^{-1} sr^{-1} or 10%
Measurement Accuracy	
Flux, p+ < 100 MeV	unknown
Flux, p+ > 100 MeV	unknown
Measurement Uncertainty - Energy	< 20%

5.8 Possible Product Improvements

The lowest energy detector is contaminated by high energy electrons. Tom Sotirelis of JHU-APL is working on an algorithm to remove this contamination.

At low L-values, where the detected ions are primarily from radiation belts, the pitch angle particle distribution should also be included in the analysis. For low pitch angles, the convolution of the pitch angle distribution function could also be included in the calculations given the magnetic field vectors needed to determine the loss cone angle and B-field pointing relative to the detectors. This overlap might be done with the use of a lookup table.

6   DETECTOR PARAMETERS

6.1 Detector effective geometric factors

The fields of view for each detector depend on the energy range as discussed by Evans and Greer (2006). The total response for each detector including FOVs was determined by GEANT4 modeling by ATC (Tom Sotirelis, JHU-APL, private communication, 7 February 2012). The GEANT4 modeling was for the three higher energy (35, 70 and 140 MeV) detectors and over a 0.5 cm^2 detector area.   The aperture was assumed to be 180˚ for the two higher energy detectors and 120˚ for the 35-MeV detector. The particles were assumed to come isotropically from 180˚. The form of the effective geometric factors for one detector is a plateau at low energy (where the height represents the FOV and a detector efficiency of nearly 1) and a fall off at higher energies. For this algorithm, the effective geometric factors were roughly fit to power law functions using the GEANT4 data. The error in these fits was about 20%.

For the lowest energy detector (16 MeV), we assumed that plateau height was the same as for detector 1 (35 MeV).   The power law exponent for detector 0 was taken to be the average of the exponents for the other three detectors.

These values may be updated in future software versions.

Table 12.   Power law fits of the form $g_{0i} E^{\delta}$ for the effective geometric factors for detectors obtained from GEANT4 modeling.

detector	energy range(MeV)	$g_{0i} E^{\delta}$
3	140-250	$5225.2\ E^{-1.5487}$
2	70-250	$488.5\ E^{-1.2383}$
1	90-250	$618.89\ E^{-1.3469}$
	35-90	1.4
0	50-250	$327\ E^{-1.38}$
	16-50	1.4

7   Software

7.1 Code package

The code is written in C. The main program is omni_flux.c. There are two versions of the wrapping program. For test purposes, one should use *omni_flux0 .c* while for operational purposes, one should follow the example of *omni_flux_calc .c*. The primary components of the code package are:

makeo   make file for *omni_flux0.c*
omni_flux0 .c   calls *omni_flux* and contains needed #defines etc.
omni_flux_calc .c   same as *omni_flux0.c* but without test routines
omni_flux.h   defines output structure
omni_testdata.txt   test data for *omni_flux0.c*
omni_out_master.txt   file should match *omni_out.txt* when *omni_flux0* is run with ITEST=1

In *omni_flux.c*, the primary flags are
isimple   0: do a regular fit; 1: do a simple fit
iskip   0: proceed with fit; 1: set all parameters to -999

The primary flow of *omni_flux.c* is as follows

init()   initialize variables

init_flags()   initialize variables
                                 set *iskip* or *isimple* to 1 based on *omni*[]

if *iskip*=0
  mk_cn()   create not overlapping count rates in *cn*[]
                                 set *iskip* or *isimple* to 1 if problems

if *iskip*=0 and *isimple*=0
  pl_fit()   do piecewise power law fit to data
                                 set *isimple*=1 if problems with fit

if *iskip*=0 and *isimple*=1
  mk_simple()   do simple fit with one power law fit to data

mk_output()   copy output into output structure
                                 if *iskip*=1, *flag_fit*=-1 and output set to -999

7.2 Test data

The test data is in *omni_testdata.txt.* To run the test data, set *ITEST*=1 in *omni_flux0.c.* The program will produce an output file *omni_out.txt* which should be identical with *omni_out_master.txt*.
As of 27 March 2012, the test data file contained:

```
11          number_of_recs
10000.0 500.0 20.0 2.0
1000.0 200.0 80.0 24.0
25.0 5.0 2.0 1.0
12.0 10.0 1.0 0.0
5.0 8.8 8.0 7.0
-6.0 1.0 2.0 3.0
23.0 2.0 2.0 0.0
80.0 2.0 2.0 2.0
16.0 6.0 8.0 0.0
16.0 26.0 8.0 0.0
1.0 0.0 0.0 1.0
```

The corresponding output file contained:

```
rec: 0                    omni: 10000, 500, 20, 2        err:  0.29
fit type: 0               flags: 0 0 0 0 0          version: 1.0
Eedge1: 16 46 91 250      jout: 248.453 7.656 0.084
gamma: -4.8 -6.5 -3.9     jf0: 1.41504e+09 8.96382e+11 8.10052e+06

rec: 1                    omni: 1000, 200, 80, 24        err:  0.29
fit type: 0               flags: 0 0 0 0 0          version: 1.0
Eedge1: 16 49 96 250      jout: 29.218 3.609 0.503
gamma: -3.0 -2.8 -2.3     jf0:   494406    243295     17085

rec: 2                    omni: 25, 5, 2, 1          err:  0.77
fit type: 0               flags: 0 0 0 0 0          version: 1.0
Eedge1: 16 49 96 250      jout: 0.732 0.089 0.012
gamma: -3.0 -2.9 -1.3     jf0:   13154.2   8850.24   4.26095

rec: 3                    omni: 12, 10, 1, 0          err:  1.02
fit type: 1               flags: 0 0 0 0 0          version: 1.0
Eedge1: 16 49 99 250      jout: 0.885 0.119 0.016
gamma: -2.9 -2.9 -2.9     jf0:    10021     10021     10021

rec: 4                    omni: 5, 9, 8, 7          err:  1.02
fit type: 1               flags: 0 0 0 0 0          version: 1.0
Eedge1: 16 49 99 250      jout: 0.339 0.045 0.006
gamma: -2.9 -2.9 -2.9     jf0:   3833.84   3833.84   3833.84

rec: 5                    omni: -6, 1, 2, 3          err:  -999.00
fit type:-1               flags: 0 1 0 0 0          version: 1.0
Eedge1: -999 -999 -999 -999    jout: -999.000 -999.000 -999.000
gamma: -999.0 -999.0 -999.0    jf0:     -999      -999      -999
```

```
rec: 6                          omni: 23, 2, 2, 0           err:  1.02
fit type: 2                      flags: 0 0 1 1 1           version: 1.0
Eedge1: 16 49 99 250      jout: 0.756 0.020 0.001
gamma: -5.3 -5.3 -5.3      jf0: 1.72642e+07 1.72642e+07 1.72642e+07

rec: 7                          omni: 80, 2, 2, 2           err:  1.02
fit type: 2                      flags: 0 0 0 1 0           version: 1.0
Eedge1: 16 49 99 250      jout: 2.527 0.017 0.000
gamma: -7.3 -7.3 -7.3      jf0: 3.51854e+10 3.51854e+10 3.51854e+10

rec: 8                          omni: 16, 6, 8, 0           err:  1.02
fit type: 2                      flags: 0 0 1 1 1           version: 1.0
Eedge1: 16 49 99 250      jout: 0.425 0.030 0.002
gamma: -3.8 -3.8 -3.8      jf0:  95562.3  95562.3  95562.3

rec: 9                          omni: 16, 26, 8, 0          err:  1.02
fit type: 1                      flags: 0 0 0 0 0           version: 1.0
Eedge1: 16 49 99 250      jout: 1.996 0.267 0.036
gamma: -2.9 -2.9 -2.9      jf0:  22598.6  22598.6  22598.6

rec: 10                         omni: 1, 0, 0, 1            err:  1.02
fit type: 1                      flags: 0 0 0 0 0           version: 1.0
Eedge1: 16 49 99 250      jout: 0.026 0.003 0.000
gamma: -2.9 -2.9 -2.9      jf0:   294.76   294.76   294.76
```

The successful fits (fit types 0,1, or 2) from the test data are plotted in Figure 10.
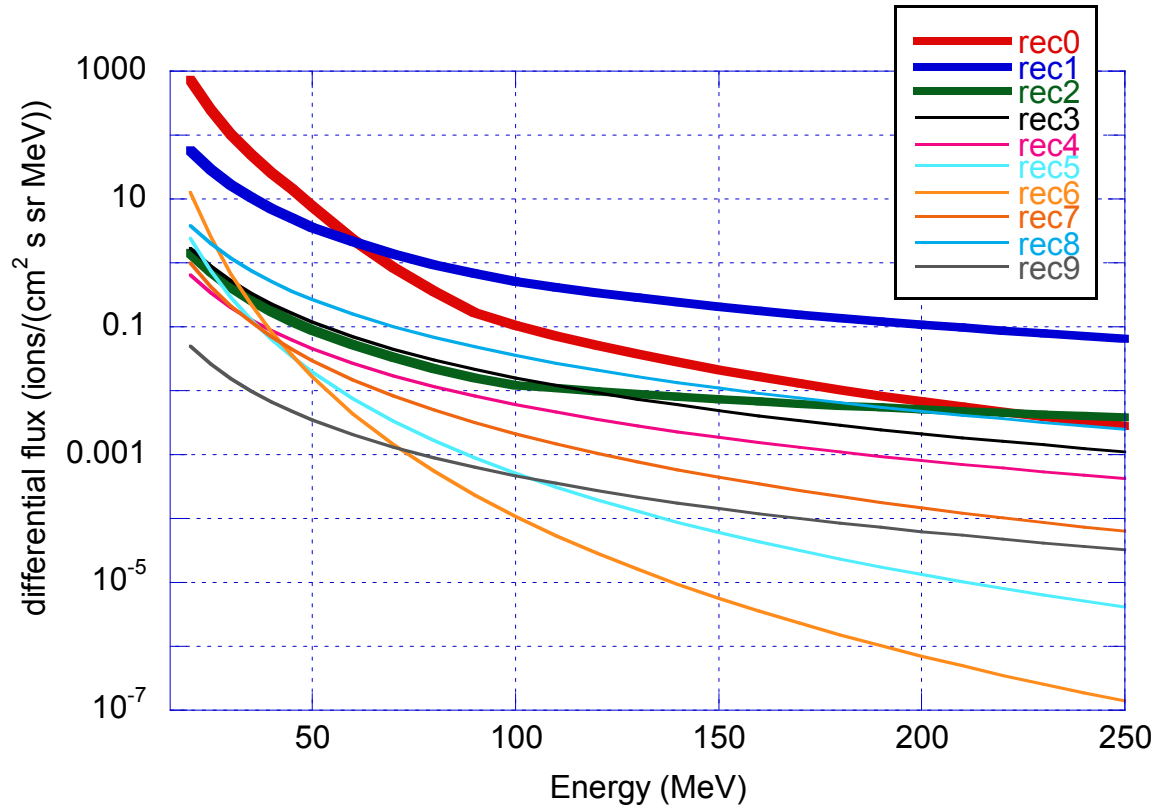
Figure 10. Plot of the successful fits from the test data. Bold curves are for cases which used piecewise power law fits.

References

Baker, D. N. (1996), Solar wind-magnetosphere drivers of space weather, *J. Atmos. Terr. Phys., 58*, 1509-1526.

Baker, D. N., R. D. Belian, P. R. Higbie, and E. W. Hones, Jr. (1979), High-energy magnetospheric protons and their dependence on geomagnetic and interplanetary conditions, *J. Geophys. Res., 84*, 7138-7154.

Bryant, D. A., T. L. Cline, U. D. Desai, and F. B. McDonald (1962), Explorer 12 observations of solar cosmic rays and energetic storm particles after the solar flare of September 28, 1961, *J. Geophys. Res., 67*, 4983-5000.

Cane, H. V., and D. Lario (2006), An introduction to CMEs and energetic particles, *Space Sci. Rev., 123*, 45-56.

Evans, D., H. Garrett, I. Jun, R. Evans and J. Chow (2008), Long-term observations of the trapped high-energy proton population (L<4) by the NOAA Polar Orbiting Environmental Satellites (POES), *Advances in Space Research, 41*, pp. 1261-1268.

Evans, D. S. and M.S. Greer (2006), Polar Orbiting Environmental Satellite Space Environment Monitor – 2: Instrument Descriptions and Archive Data Documentation, available from NGDC. (http://ngdc.noaa.gov/stp/satellite/poes/documentation.html).

Rodriguez, J., L. Mayer, T. Onsager, J. Gannon (2009), *SEISS Integral Flux Algorithm Theoretical Basis Document*, version 1.0.

Lario, D., and R. B. Decker, The energetic storm particle event of October 20, 1989, *Geophys. Res. Lett,.* 29, 10.1029/2001GL014017, 1002.

Lorentzen, K. R., J. E. Mazur, M. D. Looper, J. F. Fennell, and J. B. Blake (2002), Multisatellite observations of MeV ion injections during storms, *J. Geophys. Res.*, 107(A9), 1231, doi:10.1029/2001JA000276.

Mewaldt, R. A., C. M. S. Cohen, A. W. Labrador, R. A. Leske, G. M. Mason, M. I. Desai, M. D. Looper, J. E. Mazur, R. S. Selesnick, and D. K. Haggerty (2005), Proton, helium, and electron spectra during the large solar particle events of October–November 2003, *J. Geophys. Res., 110*, A09S18, doi:10.1029/2005JA011038.

Sauer, H. H., and D. C. Wilkinson (2008), Global mapping of ionospheric HF/VHF radio wave absorption due to solar energetic protons, *Space Weather,* 6, 10.1029/2008SW000399.